A generalized noise variance analysis model and its application to the characterization of 1/f noise

Emily J. McDowell[1], Xiquan Cui[2], Zahid Yaqoob[2], and Changhuei Yang[1, 2]

[1]Department of Bioengineering (MC138-78), [2]Department of Electrical Engineering (MC 136-93), California Institute of Technology, Pasadena, CA, 91125

emilymcd@caltech.edu

Abstract: We present a novel generalized model for the analysis of noise with a known spectral density. This model is particularly appropriate for the analysis of noise with a $1/f^{\alpha}$ distribution. The noise model reveals that, for $\alpha>1$, $1/f^{\alpha}$ noise significantly impacts the signal-to-noise ratio (SNR) for integration times that near a characteristic time, beyond which the SNR will no longer significantly improve with increasing integration time. We experimentally verify our theoretical findings with a set of experiments employing a quadrature homodyne optical coherence tomography (OCT) system and find good agreement. The characteristic integration time is measured to be approximately 2 ms for our system. Additionally, we find that the 1/f noise characteristics, including the exponent, α, as well as the characteristic integration time, are system and photodetector dependent.

OCIS codes: (120.3180) Interferometry; (110.4280) Noise in imaging systems; (170.4500) Optical coherence tomography; (170.3880) Medical and biological imaging.

References and links

1. P. Dutta and P. M. Horn, "Low-frequency fluctuations in solids - 1/f noise," Rev. Mod. Phys. **53**, 497 516 (1981).
2. W. H. Press, "Flicker noises in astronomy and elsewhere," Comments Astrophys. **7**, 103-119 (1978).
3. M. B. Weissman, "1/f noise and other slow, nonexponential kinetics in condensed matter," Rev. Mod. Phys. **60**, 537-571 (1988).
4. W. T. Li and D. Holste, "Universal 1/f noise, crossovers of scaling exponents, and chromosome-specific patterns of guanine-cytosine content in DNA sequences of the human genome," Phys. Rev. E **71**, 041910 (2005).
5. R. F. Voss, "Linearity of 1/f noise mechanisms," Phys. Rev. Lett. **40**, 913-916 (1978).
6. P. C. Ivanov, L. A. N. Amaral, A. L. Goldberger, S. Havlin, M. G. Rosenblum, H. E. Stanley, and Z. R. Struzik, "From 1/f noise to multifractal cascades in heartbeat dynamics," Chaos **11**, 641-652 (2001).
7. T. Musha and H. Higuchi, "1/f fluctuation of a traffic current on an expressway," Jpn. J. Appl. Phys. **15**, 1271-1275 (1976).
8. E. Milotti, "1/f noise: A pedagogical review," invited talk to E-GLEA-2 (2001).
9. B. Kaulakys, V. Gontis, and M. Alaburda, "Point process model of 1/f noise vs a sum of lorentzians," Phys. Rev. E **71**, 051105 (2005).
10. J. B. Johnson, "The schottky effect in low frequency circuits," Phys. Rev. **26**, 0071-0085 (1925).
11. W. Schottky, "Small-shot effect and flicker effect," Phys. Rev. **28**, 74-103 (1926).
12. Z. Siwy and A. Fulinski, "Origin of 1/f(alpha) noise in membrane channel currents," Phys. Rev. Lett. **89**, (2002).
13. D. Huang, E. A. Swanson, C. P. Lin, J. S. Schuman, W. G. Stinson, W. Chang, M. R. Hee, T. Flotte, K. Gregory, C. A. Puliafito, and J. G. Fujimoto, "Optical coherence tomography," Science **254**, 1178-1181 (1991).
14. A. M. Rollins and J. A. Izatt, "Optimal interferometer designs for optical coherence tomography," Opt. Lett. **24**, 1484-1486 (1999).
15. J. R. Barry and E. A. Lee, "Performance of coherent optical receivers," Proc. IEEE **78**, 1369-1394 (1990).
16. S. D. Personic, "Image band interpretation of optical heterodyne noise," AT&T Tech. J. **50**, 213 (1971).
17. L. G. Kazovsky, "Optical heterodyning versus optical homodyning: A comparison," J. Opt. Commun. **6**, 18-24 (1985).
18. V. Greco, C. Iemmi, S. Ledesma, A. Mannoni, G. Molesini, and F. Quercioli, "Multiphase homodyne displacement sensor," Optik **97**, 15-18 (1994).

#78143 - $15.00 USD Received 18 December 2006; revised 13 March 2007; accepted 13 March 2007

19. X. Q. Liu, W. Clegg, D. F. L. Jenkins, and B. Liu, "Polarization interferometer for measuring small displacement," IEEE Trans. Instrum. Meas. **50**, 868-871 (2001).
20. C. M. Wu, C. S. Su, G. S. Peng, and Y. J. Huang, "Polarimetric, nonlinearity-free, homodyne interferometer for vibration measurement," Metrologia **33,** 533-537 (1996).
21. C. Chao, Z. H. Wang, W. G. Zhu, and O. K. Tan, "Scanning homodyne interferometer for characterization of piezoelectric films and microelectromechanical systems devices," Rev. Sci. Instrum. **76,** 063906 (2005).
22. D. L. Mazzoni and C. C. Davis, "Trace detection of hydrazines by optical homodyne interferometry," Appl. Opt. **30,** 756-764 (1991).
23. E. Beaurepaire, L. Moreaux, F. Amblard, and J. Mertz, "Combined scanning optical coherence and two-photon-excited fluorescence microscopy," Opt. Lett. **24,** 969-971 (1999).
24. M. A. Choma, C. H. Yang, and J. A. Izatt, "Instantaneous quadrature low-coherence interferometry with 3 x 3 fiber-optic couplers," Opt. Lett. **28,** 2162-2164 (2003).
25. Z. Yaqoob, J. Fingler, X. Heng, and C. Yang, "Homodyne en face optical coherence tomography," Opt. Lett. **31,** 1815-1817 (2006).
26. N. Choudhury, G. J. Song, F. Y. Chen, S. Matthews, T. Tschinkel, J. F. Zheng, S. L. Jacques, and A. L. Nuttall, "Low coherence interferometry of the cochlear partition," Hearing Res. **220,** 1-9 (2006).
27. R. Leitgeb, C. K. Hitzenberger, and A. F. Fercher, "Performance of Fourier domain vs. time domain optical coherence tomography," Opt. Express **11,** 889-894 (2003).
28. M. A. Choma, M. Sarunic, C. Yang, and J. A. Izatt, "Sensitivity advantage of swept source and Fourier domain optical coherence tomography," Opt. Express **11,** 2183 - 2189 (2003).
29. J. F. de Boer, C. B., B. Park, M. Pierce, G. Tearney, and B. Bouma, "Improved signal-to-noise ratio in spectral-domain compared with time-domain optical coherence tomography," Opt. Lett. **28,** 2067 -2069 (2003).
30. Y. Salvade and R. Dandliker, "Limitations of interferometry due to the flicker noise of laser diodes," J. Opt. Soc. Am. A **17,** 927-932 (2000).
31. R. H. Hamstra and P. Wendland, "Noise and frequency-response of silicon photodiode operational amplifier combination," Appl. Opt. **11,** 1539 (1972).
32. J. Clarke and T. Y. Hsiang, "Low-frequency noise in tin and lead films at superconducting transition," Phys. Rev. B **13,** 4790-4800 (1976).
33. M. S. Keshner, "1/f noise," Proc. IEEE **70,** 212-218 (1982).
34. B. Pellegrini, R. Saletti, P. Terreni, and M. Prudenziati, "1/f-gamma noise in thick-film resistors as an effect of tunnel and thermally activated emissions, from measures versus frequency and temperature," Phys. Rev. B **27,** 1233-1243 (1983).
35. M. A. Caloyannides, "Microcycle spectral estimates of 1/f noise in semiconductors," J. Appl. Phys. **45,** 307-316 (1974).
36. B. B. Mandelbrot and J. R. Wallis, "Some long-run properties of geophysical records," Water Resources Research **5,** 321 (1969).
37. A. Yariv and P. Yeh, *Photonics: Optical electronics in modern communications* (Oxford University Press, New York, 2007).

1. Introduction

1/f noise, alternately referred to as pink or flicker noise, is found in a wide range of physical systems [1-4], from carbon resistors and semiconductors [5], to heartbeat dynamics [6] and traffic flow [7]. In general, 1/f noise has a power spectral density that follows the form $1/f^{\alpha}$, where α commonly ranges from 0.5 to 1.5 [8]. Despite significant effort in describing a universal model for the origin of 1/f noise [9], no single model is currently accepted, and the origins of 1/f noise have only been well characterized in very specific circumstances. For example, 1/f noise in vacuum tubes is commonly modeled as a superposition of relaxation rates that characterize the release of electrons from cathode surface trapping sites [8, 10, 11]. Additionally, the 1/f noise measured in cellular ion currents has been attributed to the stochastic nature of the opening and closing mechanisms of voltage gated ion channels [12].

The presence of 1/f noise in optical detection can significantly degrade the effective precision and sensitivity of the optical technique. In interferometric methods, including time domain optical coherence tomography (OCT) [13], a typical strategy for avoiding 1/f noise involves the use of heterodyne detection in which the signal of interest is modulated and shifted into a frequency band in which 1/f noise is small compared to other sources of noise. Under these circumstances, we typically consider only white noise processes which include receiver noise, shot noise, and excess intensity noise [14].

Homodyne methods are advantageous in their simplicity. By directly detecting the interferometric signal, there is no need for scanning mechanisms or lock-in detection. In addition, a properly performed homodyne experiment can provide a 3 dB improvement in

#78143 - $15.00 USD Received 18 December 2006; revised 13 March 2007; accepted 13 March 2007

SNR compared to heterodyne techniques [15-17]. Homodyne interferometric methods have long been used to measure displacements [18, 19] and vibrations [20, 21], and have been adapted to a variety of other applications including the detection of trace gasses [22]. In addition, there is a recent rise in homodyne interferometric methods for biomedical applications [23-26]. We also note that most of the spectrometer-based OCT systems reported thus far, which have an improved SNR over time domain techniques [27-29], are homodyne in nature. An understanding of the impact of 1/f noise can guide better detection scheme design, and direct the selection of operating parameters.

The issue of 1/f noise in homodyne detection, and optical detection in general, is an understudied problem. In an optical system, we expect 1/f noise to be generated by the broadband source [30], as well as the photodetector circuitry [31]. The complex nature of the light detection process makes it difficult to directly identify the specific noise generating sources in the light detection chain. More importantly, even if the 1/f noise characteristics of a given system can be empirically determined, there is a need for a suitable theoretical model that can be used to characterize the impact of 1/f noise on the sensitivity of a detection system.

In Section 2, we present a novel time domain approach to determine the SNR behavior of an optical system in the presence of 1/f noise. To our knowledge, this approach has not been previously reported. Using this model, we examine the impact of the noise exponent, α, (Section 2.1) as well as the total experimental time frame, T (Section 2.2). Two findings are particularly noteworthy. 1) The noise model shows that for $\alpha>1$, the 1/f noise variance is proportional to the square of the integration time (τ). This implies that for measurements that are dominated by 1/f noise, the SNR can not be improved by increasing the integration time of the measurement. 2) The noise model also predicts the existence of a characteristic time ($\tau_{white\text{-}to\text{-}1/f}$) at which 1/f noise begins to dominate over white noise, such as shot noise. In Section 3, we describe our 3x3 fiber coupler based homodyne interferometer, as well as the experiments that were conducted to characterize 1/f noise in that system. In Section 4, we compare our theoretical results to experimental findings from the homodyne interferometer. In addition to validating our theoretical results, we also find that the 1/f noise characteristics are detector dependent. Finally, we summarize our findings in Section 5.

2. Theoretical noise model

In the following analysis we will consider a generalized noise source with known power spectral density. It is a well known fact that SNR in the limit of dominant white noise, such as shot noise, increases linearly with integration time (τ). (In keeping with interferometry convention, we define SNR as the ratio of the square of the signal count to the noise variance.) However, we do not expect this trend in the case of dominant 1/f noise. The presence of 1/f noise implies that the amplitude of noise fluctuations will increase on longer time scales. The following model allows us to examine the dependence of both 1/f noise and white noise on integration time, and determine the appropriate detection parameters to obtain the optimal SNR for a given optical system.

In order to determine the contribution of 1/f noise to the SNR of an optical system, we would like to determine the variance of the 1/f noise amplitude distribution as a function of the integration time of the detection system. The following derivation presents a method for determining this variance using the power spectral density of the noise to construct a time series that can then be ensemble averaged appropriately. This is, to the best of our knowledge, a new approach that is useful for analyzing any generalized noise sources for which the power spectral density is known. For the sake of clarity, we choose to quantify our signal in terms of photon count rate and photon counts. We note that through appropriate scaling these expressions can be converted to quantities of energy and power.

We can describe the signal time trace as a combination of a DC term, representing the mean signal, and a time varying, zero mean term that represents the noise. The noise term can be expressed as a summation of frequency dependent contributions, each weighted by the power spectral density of the noise distribution:

#78143 - $15.00 USD Received 18 December 2006; revised 13 March 2007; accepted 13 March 2007

$$x(t) = x_0 + \Delta x(t)$$
$$= x_0 + \sum_{i=1}^{\infty} \sqrt{2S(f_i)\Delta f}\,\cos(2\pi f_i t + \delta_i) \tag{1}$$

Here, x_0 is the mean signal (photon count rate), $S(f_i)$ is the power spectral density corresponding to the frequency f_i, and δ_i is a random phase shift that varies uniformly on the interval $[0, 2\pi]$. The phase shifts between f_i and f_{i+1} are uncorrelated, producing the desired noise source. The exact definition of the power spectral density, $S(f)$, can vary from community to community. The power spectral density employed here is given by the Fourier transform of autocorrelation function of the measured signal. This results in a symmetrically distributed power spectrum. $S(f)$ in Eq. (1) is a single sided power spectrum, which contains double the original value for each positive frequency. The power contained in each frequency step, Δf, is given by $S(f)\Delta f$. Thus, to obtain the total signal in each frequency step we must include the discretization within the square root in Eq. (1). We briefly verify our representation of the signal in Eq. (1) by noting that for a signal of the form $A\cos(2\pi f_0 t)$, the single sided power spectrum is given by $S(f) = (A^2/2)\delta(f-f_0)$. As such, the factor $\sqrt{(2S(f)\Delta f)}$ yields the correct weight of A in the frequency step containing f_0.

An actual measurement of the signal count, which necessitates the collection of signal photons over a finite measurement time window, τ, will yield two terms. The first term simply integrates over τ to give an expected value of $X(\tau) = x_0\tau$. For the second term we have the following:

$$\Delta X(\tau) = \int_0^{\tau} \Delta x(t)\,dt \tag{2a}$$

$$E(\Delta X(\tau)) = 0 \tag{2b}$$

where the expected value of the noise fluctuations is zero. Thus, the variance of the noise is given by the second moment of $\Delta X(\tau)$:

$$\sigma_X^2(\tau) = E\left(\Delta X(\tau)^2\right) = E\left(\left[\int_0^{\tau}\left(\sum_{i=1}^{\infty}\sqrt{2S(f_i)\Delta f}\,\cos(2\pi f_i t + \delta_i)\right)dt\right]^2\right) \tag{3}$$

We can then rewrite the product,

$$\sigma_X^2(\tau) = E\left(\left[\int_0^{\tau}\sum_{i=1}^{\infty}\sqrt{2S(f_i)\Delta f}\,\cos(2\pi f_i t + \delta_i)dt\right]\left[\int_0^{\tau}\sum_{j=1}^{\infty}\sqrt{2S(f_j)\Delta f}\,\cos(2\pi f_i t + \delta_j)dt\right]\right) \tag{4}$$

noting that since δ_i and δ_j are uncorrelated for $i \neq j$, the expectation will vanish unless $i=j$.

$$\sigma_X^2(\tau) = E\left(\sum_{i=1}^{\infty}\left[\int_0^{\tau}\sqrt{2S(f_i)\Delta f}\,\cos(2\pi f_i t + \delta_i)dt\right]^2\right)$$
$$= E\left(\sum_{i=1}^{\infty}\left[\frac{\sqrt{2S(f_i)\Delta f}}{2\pi f_i}\left(\sin(2\pi f_i \tau + \delta_i) - \sin(\delta_i)\right)\right]^2\right) \tag{5}$$

#78143 - $15.00 USD Received 18 December 2006; revised 13 March 2007; accepted 13 March 2007

$$= E\left(\sum_{i=1}^{\infty} \frac{2S(f_i)\Delta f}{(2\pi f_i)^2} \left[\sin^2(2\pi f_i \tau + \delta_i) - 2\sin(2\pi f_i \tau + \delta_i)\sin(\delta_i) + \sin^2(\delta_i) \right] \right)$$

The expectation can then be evaluated by taking an ensemble average where δ_i is varied in the interval $[0, 2\pi]$.

$$\sigma_X^2 = \frac{1}{2\pi} \int_o^{2\pi} \left(\sum_{i=1}^{\infty} \frac{S(f_i)\Delta f}{2(\pi f_i)^2} \left[\sin^2(2\pi f_i \tau + \delta_i) - 2\sin(2\pi f_i \tau + \delta_i)\sin(\delta_i) + \sin^2(\delta_i) \right] \right) d\delta_i \quad (6)$$

Finally, we decrease the spacing between subsequent elements in the infinite sum, and rewrite the variance in integral form.

$$\sigma_X^2(\tau) = \int_0^{\infty} \frac{S(f)}{2(\pi f)^2} [1 - \cos(2\pi f \tau)] df \quad (7)$$

This expression is useful and generalized. It can be used with any noise power spectral density to derive the noise variance.

To verify our result, we begin by considering the situation where white noise dominates (i.e. $S(f)=A_{white}$). In this situation, Eq. (7) can be rewritten as:

$$\sigma_{X,white}^2(\tau) = \int_0^{\infty} \frac{A_{white}}{2(\pi f)^2} [1 - \cos(2\pi f \tau)] df \quad (8)$$

$$\sigma_{X,white}^2(\tau) = \frac{A_{white}\tau}{2} \quad (9)$$

Here, we can immediately recognize this form as the variance of white noise. For an idealized photon flow that is shot noise limited, the coefficient A_{white} is given by $2x_0$. This leads to $\sigma_{X,shot\ noise}^2(\tau) = x_o\tau$; a result that is consistent with the Poissonian nature of shot noise.

If we instead substitute the power spectral density that we expect for 1/f noise, $S(f)=A_{pink}/f^{\alpha}$, we obtain Eq. (10). However, this integral diverges at $f=0$. By integrating from a minimum frequency, f_{min}, we can effectively cap the function and force the integral to converge. As we will show in section 2.1, this truncation is valid under certain experimental conditions, and f_{min} is directly related to the total time frame of the experiment (T). The variance is then given by:

$$\sigma_{X,pink}^2(\tau, f_{\min}) = \int_{f_{\min}}^{\infty} \frac{A_{pink}}{2\pi^2 f^{\alpha+2}} [1 - \cos(2\pi f \tau)] df \quad (10)$$

In the following sections we analyze Eq. (10) in terms of its dependence on both f_{min} and α. Additionally, since there is no straightforward analytical solution to Eq. (10), we approximate the solution in order to show the form of the dependence on integration time (τ).

2.1 Choice of f_{min}

In our analysis, we choose $f_{min}=1/T$, where T is the total experimental time frame. This is different from the integration time τ, which gives the time step over which the signal is sampled. The difference between these two time constants can be better appreciated in the following scenario. Suppose we have a light source with a known 1/f noise power spectrum, $S(f)$, which we decide to amplitude modulate in order to send a message. The message length is T in its entirety. The message is analog in nature but is band limited such that it does not contain frequency components beyond f_{signal}. The message can be received, with no

#78143 - $15.00 USD Received 18 December 2006; revised 13 March 2007; accepted 13 March 2007

information loss, by measuring the light intensity over a time frame of T and choosing a time step of $\tau=2/f_{signal}$ for signal integration. Intuitively, we can appreciate that this time step integration is useful for suppressing high frequency ($f>f_{signal}$) noise contributions in our measurements. The noise variance for this experiment can be calculated using Eq. (10) based

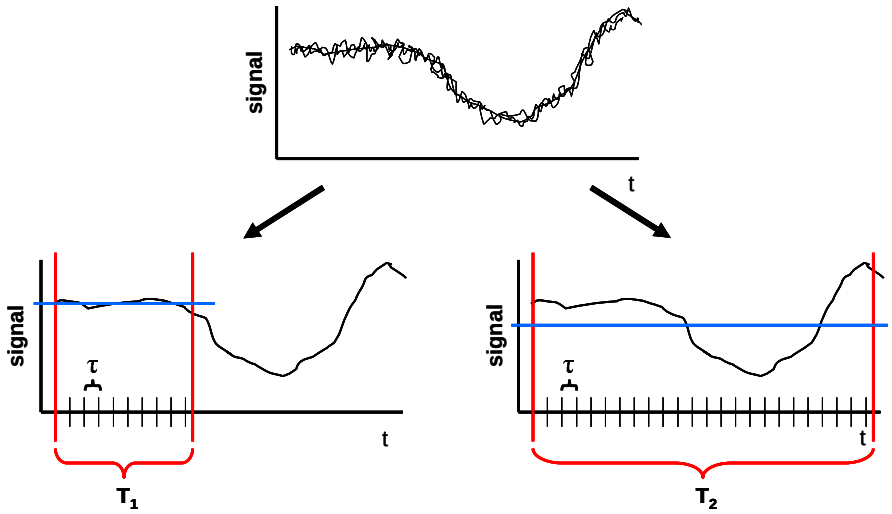

Fig. 1. The total time frame of an experiment, T, determines the lowest frequency noise components that are incorporated into a measured signal. The upper panel depicts the raw signal, or amplitude modulated 'message' that is encoded on a 1/f noise dominated light source (see Section 2.1). If the message is band limited such that it does not contain frequency components beyond f_{signal}, the message can be optimally collected by integrating the collected signal in times steps of $\tau=2/f_{signal}$. In the left panel, low frequency noise ($f<f_{min}$) in the light source causes a net DC shift in the acquired signal. As T is increased (right panel) the same low frequency noise dramatically impacts the measured noise variance between subsequent time steps (τ), which can lead to a degradation in the SNR of the collected message.

on the abovementioned parameters. We can see that the message length T is relevant for noise variance consideration; as the length of T is increased, more low frequency noise components will be incorporated, and the SNR will correspondingly deteriorate. Noise components of frequency lower than f_{min} are present in the collected signal trace. However, these components are manifested as a net DC shift in the entire collected signal, and have no impact on the content of the sent message (see Fig. 1).

There is an additional scenario in which a minimum frequency may be imposed on Eq. (10). In certain situations the power law behavior of 1/f noise breaks down for very low frequencies [8]. This imposes a natural cap on Eq. (10), which is approximately constant across these low frequencies, implying that fluctuations do not become infinitely large. In this case however, we cannot approximate Eq. (10) by simply integrating from the corner frequency through infinity. We must also consider the area under the constant portion of the power spectrum in determining the total noise variance (so long as these frequencies fall above the f_{min} imposed by the detection system). In reality, this type of natural capping has only been seen in very few experimental situations [32, 33]. Most often, 1/f behavior can be seen down to the lower frequency bound of the measurement. In fact, 1/f noise has been measured over 6 frequency decades [34], and has been shown to display the familiar trend at frequencies as low as 1/(3 weeks) in MOSFETs [35] and even 1/(300 years) for weather data [36].

2.2 Influence of the noise exponent, α

The value of α can dramatically influence the 1/f noise variance characteristics. To motivate our discussion, we will first present numerical solutions to Eq. (10), allowing for an empirical

#78143 - $15.00 USD Received 18 December 2006; revised 13 March 2007; accepted 13 March 2007

determination of the dependence on integration time. For verification, we will more rigorously demonstrate the τ dependence by deriving an approximation to Eq. (10), which clearly reveals the role of τ.

Equation (10) is numerically approximated (MATLAB), and the standard deviation of the noise fluctuations (square root of Eq. 10) is plotted in Fig. 2 for various values of α. These curves are solely intended for the purpose of examining the dependence of the noise on integration time. The individual curves plotted in Fig. 2 have arbitrary amplitudes relative to one another, as the units of A_{pink} will change as α is varied. A f_{min} of 1.6 mHz, corresponding to a relatively long experimental time frame, was used in these simulations.

As we expect, the white noise curve, α=0 in Figs. 2(a) -2(b) show a dependence on the square root of the integration time. As α varies from 0 to 1 [Fig. 2(a)], the standard deviation appears to transition from a square root - type dependence towards a linear dependence. This response demonstrates the gradual transition from white noise to 1/f noise as α is increased. Interestingly, for α>1 [Fig. 2(b)], the standard deviation appears to increase linearly with integration time. This suggests the fact that, under conditions where 1/f noise is dominant, the total noise increases in proportion with the signal. Additionally, we note that the white noise curve tapers faster than all curves for which $\alpha \neq 0$. Thus, each of the 1/f noise curves necessarily crosses the shot noise curve at some point. This fact implies the existence of a characteristic time ($\tau_{white\text{-}to\text{-}1/f}$) at which 1/f noise begins to dominate over white noise.

SNR traces corresponding to the same α values as Fig. 2 are plotted in Fig. 3. Here, we define SNR as $(X/\sigma)^2$ [37], where X is the total number of photon counts, which increases linearly with τ, and σ is the standard deviation of the noise. As expected, the theoretical shot noise limited SNR increases linearly with integration time. For $0<\alpha<1$, the SNR transitions from a curve that is approximately linear (similar to white noise), to a curve that appears to taper towards a constant value. The linear dependence of the 1/f noise standard deviation in Fig. 2(b) implies that the corresponding SNR will be constant, since the total signal also

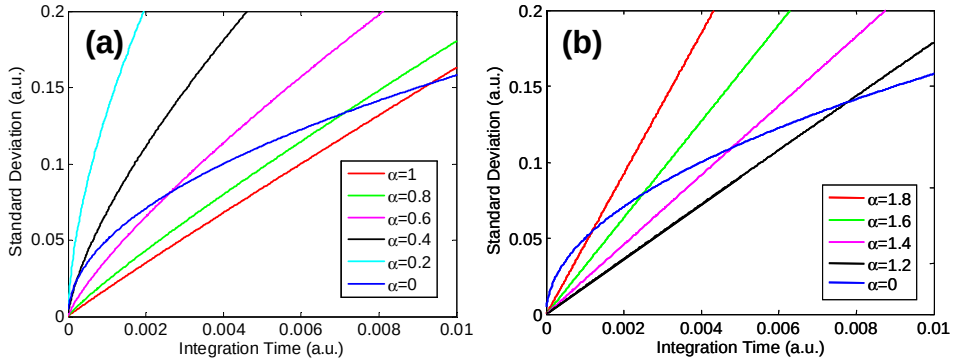

Fig. 2. Theoretical results for noise standard deviation versus integration time, square root of Eq. (9) and Eq. (10) for white noise and 1/f noise, respectively. The 1/f noise transitions from the square-root dependence of white noise (α=0) to a linear dependence as α increases from 0 to 1, and maintains a linear dependence on integration time for α>1.

#78143 - $15.00 USD Received 18 December 2006; revised 13 March 2007; accepted 13 March 2007

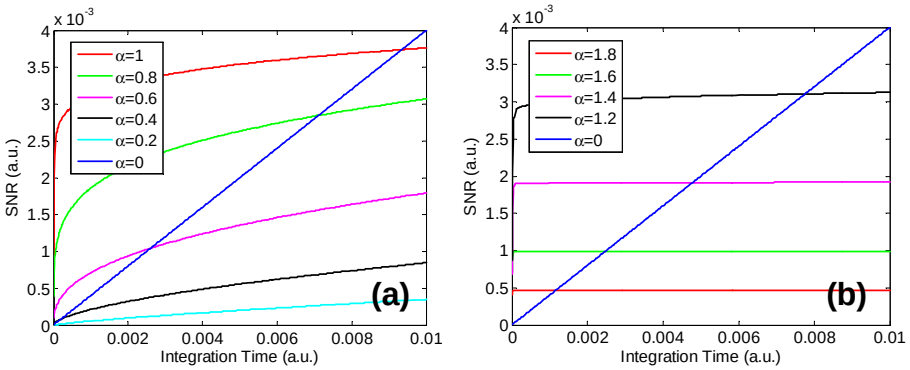

Fig. 3. Theoretical results for SNR versus integration time. As expected, the white noise limited SNR increases linearly with integration time. In the case of dominant 1/f noise, the SNR increases with decreasing slope for $0<\alpha<1$, and tapers to a constant value for $\alpha>1$.

increases linearly with increasing integration time. Figure 3(b) shows that this appears to be empirically true.

The above simulations provide some initial intuition into the dependence of integration time on SNR in the limit dominant 1/f noise. It is possible to derive an approximate solution to Eq. (10) that shows the explicit dependency of the noise variance on integration time, τ, for a wide class of experimental situations. Specifically, if $\tau << 1/f_{min}$, Eq. (10) can be easily simplified. In the context of the thought experiment described above (Section 2.1), this constraint corresponds to a situation in which the message is long (f_{min} small) and the maximum signal frequency is high ($\tau = 2/f_{signal}$ is small) – a signal that can be expected to describe an overwhelmingly large fraction of practical situations. Under these conditions, we arrive at the following expressions for the noise variance:

$$\sigma^2_{X,pink}(\tau, f_{\min}) \approx \frac{A_{pink}}{2}\left[\frac{(2\pi)^{\alpha}\tau^{\alpha+1}}{(\alpha+1)\alpha\Gamma(\alpha)\cos\left(\frac{\alpha\pi}{2}\right)}\right] \qquad 0<\alpha<1$$
$$\approx A_{pink}\left[\frac{\tau^2}{(\alpha-1)f_{\min}^{\alpha-1}}\right] \qquad \alpha>1 \qquad (11)$$
$$\text{except when } \alpha \in Z^+$$

where $\Gamma(\alpha)$ is the mathematical gamma function defined as $\int t^{\alpha-1}e^{-t}dt$ over the interval $[0,\infty]$ for $\alpha>0$. Z^+ refers to the set of positive integers. Eq. (11) shows that, for small f_{min} and increasing τ, two distinct regimes exist. In these regimes, the SNR depends on τ as follows:

$$SNR(\tau) \sim O\left(\tau^{1-\alpha}\right) \qquad 0<\alpha<1$$
$$\sim O\left(\tau^{0}\right) \qquad \alpha>1 \qquad (12)$$
$$\text{except when } \alpha \in Z^+$$

For $0<\alpha<1$ Eq. (11) shows a dependence of the variance on $\tau^{\alpha+1}$. This confirms our intuition of a transition from white noise to 1/f noise, as the SNR moves from a function with τ dependence to a function of constant value. This dependence implies that the SNR can still increase after crossing the characteristic integration time ($\tau_{white\text{-}to\text{-}1/f}$) at which 1/f noise begins to dominate, although the gain in SNR from further increases in τ occurs with diminishing returns as α approaches 1.

#78143 - $15.00 USD Received 18 December 2006; revised 13 March 2007; accepted 13 March 2007

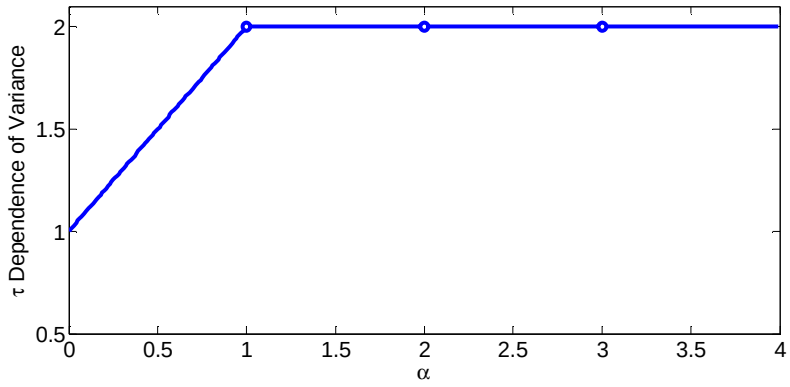

Fig. 4. The dependence of the 1/f noise variance is dependent on integration time varies with the 1/f exponent, α. For α>2, this dependence is given by τ^2. Open circles represent α values that cannot be simply approximated by Eq. (11).

For α>1 we find a τ^2 dependence. These approximations confirm our observations from Figs. 2 and 3 that, for α>1, the SNR should reach a constant value when 1/f noise is the dominant noise process. This is quite a remarkable fact, implying that once the integration time is increased past $\tau_{white\text{-}to\text{-}1/f}$, there will be no further significant improvements in SNR. The τ dependence of Eq. (10) and Eq. (11) is plotted in Fig. 4 versus the 1/f exponent, α. For integer values of α, Eq. (10) cannot be easily solved, and these locations are represented by open circles.

3. Experimental methods

The model described in Section 2 is widely applicable. In particular, it is very appropriate for determining the noise characteristics that are influential in homodyne interferometry. In the next two sections, we describe our findings for this specific application area. A 3x3 fiber coupler based homodyne optical coherence tomography system first described by Yaqoob *et al.* [25] was used to study 1/f noise and its impact in homodyne interferometry. This type of system was chosen because of its ability to instantaneously decouple phase and amplitude information [24]. Additionally, the system sensitivity does not depend on maintaining a phase difference of exactly 90°. A calibration procedure accompanied by appropriate processing allows us to relax the requirement for stringent phase control in order to use the inherent phase shifts of the fiber coupler.

Figure 5(a) shows the experimental setup utilized in this study. Broadband light from a superluminescent diode (λ_0=1300nm, $\Delta\lambda$=85nm) enters a 2x2 fiber coupler, followed by a 3x3. Backscattered light from the sample is mixed with reference light to create an interference pattern that is detected at detectors 1-3. Detector 4 is used to monitor and correct for source fluctuations. Figure 5(b) diagrams the vector relationship between the signals at each arm of the 3x3 coupler, noting the dependence on the power transfer coefficients α_{mn} of the fiber coupler. The interferometric signals are phase separated by nominally 120° (depending on the α_{mn}), as required by conservation of energy. The optical signal at the j^{th} detector is given by:

$$P_j(z) = P_{r,j} + P_{s,j} + 2(1/s_j)\sqrt{\alpha_{4,1}\alpha_{4,j}\alpha_{5,1}\alpha_{5,j}P_r}\left(\sqrt{P_s(z)} \otimes \gamma(z)\cos\left(\theta(z)+\phi_j\right)\right) \quad (13)$$

where $P_{r,j}$ and $P_{s,j}$ represent the total DC power returning from the reference and sample arms, respectively; $1/s_j$ is a scaling factor that accounts for both coupler and detector loss; P_r is the returning reference power; $P_s(z)$ is the returning coherent light from a depth z within the sample; $\gamma(z)$ is the source autocorrelation function; $\theta(z) = 2k_0z + \psi(z)$, is the phase associated

#78143 - $15.00 USD Received 18 December 2006; revised 13 March 2007; accepted 13 March 2007

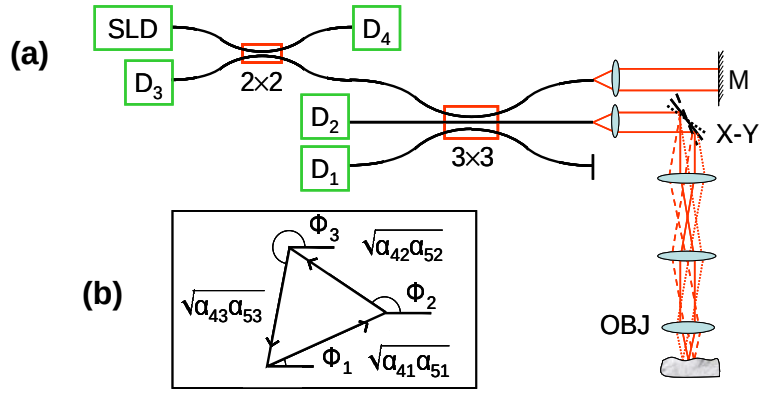

Fig. 5. (a). Schematic of 3x3 homodyne OCT system employed in this study. (b) Diagram of the vector relationship between the signals detected at ports 1-3. SLD: Superluminescent diode; D_i: ith detector; M: Mirror; X-Y: X-Y Scanner; OBJ: Microscope objective.

with each depth in the sample, where k_0 is the optical wavenumber corresponding to the center wavelength of the source and $\psi(z)$ is the intrinsic reflection phase shift of the sample at depth z; Finally, φ_j represent the phase shifts between each of the three detectors, attributable to the phase shifts inherent to the 3x3 fiber coupler. The signal of interest, which describes the reflectivity profile of the sample, is the coefficient of the cosine term, which can be isolated, after DC removal, by simply squaring and summing the signals from the three ports.

The system depicted in Fig. 5 was built and calibrated, with phase shifts measured as φ_1=116.6 ± 1.2°, φ_2=120.7 ± 0.9°, φ_3=122.5 ± 0.8°. The objective lens was a 20x, 0.4 NA IR lens, allowing for a measured lateral resolution of 9.4 μm. The broadband SLD source provided a measured axial resolution of 14 μm. A sample arm power of approximately 30 μW, measured at a single detector, was used in all following experiments. In order to experimentally measure the SNR of the homodyne interferometer, time traces of the OCT signal were acquired with a mirror in the sample arm. To measure the noise contribution, the sample arm was blocked. Varying integration times were used to bin the measured signal into integrated 'blocks'. These 'blocks' are represented in Fig. 1 by dashed lines with spacing τ, and the integrated signal is proportional to the total number of photons detected over this time interval. The power spectrum of the noise was determined using only the integrated noise signal. The SNR was determined by taking the square of the mean value of the integrated signal divided by the standard deviation of the integrated noise signal

To set a baseline for the evaluation of the effects of 1/f noise on the homodyne system, a heterodyne system was constructed and evaluated as well. The reference mirror labeled in Fig. 5 was mounted on a voice coil to allow for modulation of the reference arm optical path length. The interferometric signal was detected at a single port of the fiber coupler, and the envelope of the interferogram was acquired using a lock-in amplifier set at the Doppler shift frequency created by the velocity of the moving reference mirror. Instead of visualizing only a single point, we acquired the entire coherence function in depth as we scanned the reference arm. To measure the SNR we integrated over the central portion of the peak, defined by the full width at half maximum (FWHM), as well as over the same number of points in an area distant to the peak. The integration time was set by the width of the peak, determined by the speed at which the reference arm was scanned. By changing the scan speed, and locking in on the appropriate carrier frequency, we were able to determine the dependence of the SNR on integration time.

Finally, we were interested in investigating the source of 1/f noise in our homodyne interferometer. In order to examine the contribution of detector 1/f noise, we replaced our initial detectors (NewFocus, #2011) with new detectors (Thorlabs, #DET10C). We acquired

#78143 - $15.00 USD Received 18 December 2006; revised 13 March 2007; accepted 13 March 2007

homodyne data as described above, and compared the data sets in terms of the 1/f noise characteristics.

One potential problem that was necessary to address involved the discrete sampling of the photodetectors. We wanted to acquire data points that represented the mean signal over the time between subsequent samples, but photodiodes do not integrate over this time period. There was the potential for high frequency noise to skew the data as we integrated over various amounts of time in post processing. To solve this problem, we set the low pass cutoff frequency on the photodetectors to match our sampling rate in all experiments. Thus, fluctuations were smoothed out on the scale of the sampling time. We note that the power spectral density remains constant with or without filtering since the cutoff frequency is found at twice the maximum frequency displayed in the power spectrum.

4. Results and discussion

4.1 Measured power spectrum

We begin our investigation of 1/f noise by displaying the power spectrum of our measured homodyne noise signal averaged over 85 data sets (Fig. 6). No capping of the 1/f noise at low frequencies can be seen over our measurement range. By fitting to the linear portion of the curve, we found an exponent of α=1.39 ± 0.1. The results of the fit also gave us a value for A_{pink}, used in the above derivation. The constant value of the white noise determined A_{white}. Additionally, we note that the frequency at which white noise processes, shot noise in this case, became dominant was approximately 70 Hz.

4.2 Experimental SNR versus integration time

After measuring the SNR of the homodyne system as described above, we plotted SNR versus integration time averaged over 65 data sets in Fig. 7. Notably, for short integration times the curve was approximately linear, while for long integration times the curve was flat. This implies that white noise was initially dominant, and that 1/f noise became increasingly prominent as the integration time was increased. This behavior agrees well with the analysis described above and plotted in Figs. 2 and 3. By fitting to the linear and constant portions of the data in Fig. 7 we experimentally determined the integration time at which 1/f noise began

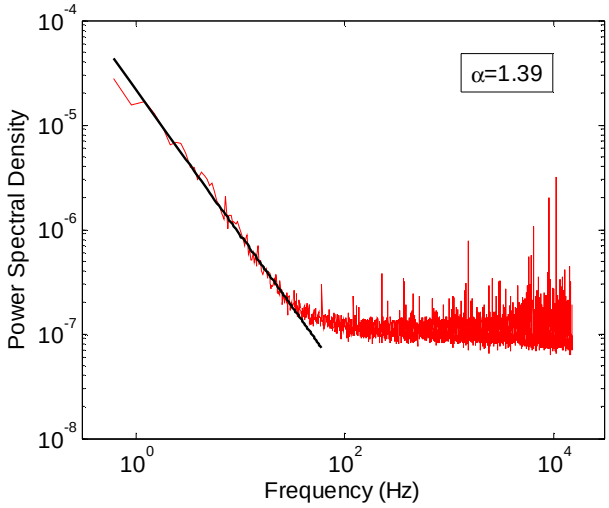

Fig. 6. Power spectral density of the interferometric noise, measured with the sample arm blocked. The data were averaged over 85 data sets, and sampled at 30 kHz. The initial portion of the curve was fit, and an exponent of α=1.39 was determined. The 1/f to white noise corner can be seen at approximately 70 Hz.

#78143 - $15.00 USD Received 18 December 2006; revised 13 March 2007; accepted 13 March 2007

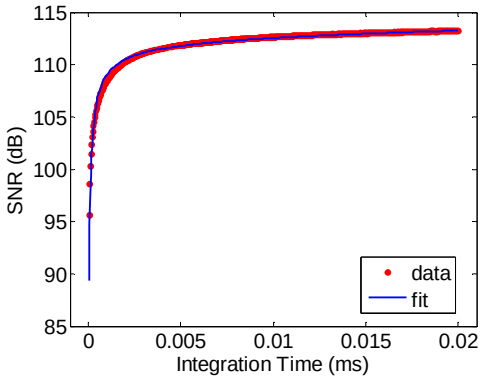

Fig. 7. SNR of the homodyne interferometric signal plotted versus integration time. The initial portion of the curve displays a linear trend, indicative of dominant white noise processes. The final portion of the curve is constant with increasing integration time, in agreement with the theorectical 1/f noise variance derived above.

to dominate as $\tau_{white\text{-}to\text{-}1/f}$ =2.1 ms. The curve was almost completely constant after several 10s of ms, and any further increase in integration time did not significantly increase the SNR. We next compared this result with those from the corresponding heterodyne system, which were collected and analyzed as described in Section 3. The use of a carrier frequency shifted our desired signal away from the baseband and out of the 1/f regime. This form of detection is the standard method employed for minimizing the contribution of 1/f noise when making electronic measurements. The stable range of voice coil frequencies, approximately 1-20 Hz, imposed the range of modulation frequencies that we were able to utilize, approximately 5-20 kHz. The voice coil frequency, directly related to the scan speed, set the width of the coherence envelope as well as the integration time of the measurement.

Figure 8 displays both heterodyne and homodyne SNR plotted on a log-log scale versus integration time. The homodyne data were averaged over 65 data sets. It is clear that the initial portion of the homodyne data falls along a line that intersects the heterodyne data at longer integration times. This is evidence confirming that the homodyne system is white noise limited for short integration times. The theoretical upper limit on SNR, when white noise is dominant, is plotted in black in Fig. 8. This upper shot noise limit assumes perfect constructive interference of the detected signal (i.e. the cosine term in Eq. (13) is always equal to 1) and the absence of other white noise sources. In principle, it is possible to reach this upper limit in homodyne detection when maintaining perfect phase control. In contrast, due to the nature of its time modulation, it is not possible to reach using heterodyne detection since we always detect the coherence function modulated by a fringe pattern.

#78143 - $15.00 USD Received 18 December 2006; revised 13 March 2007; accepted 13 March 2007

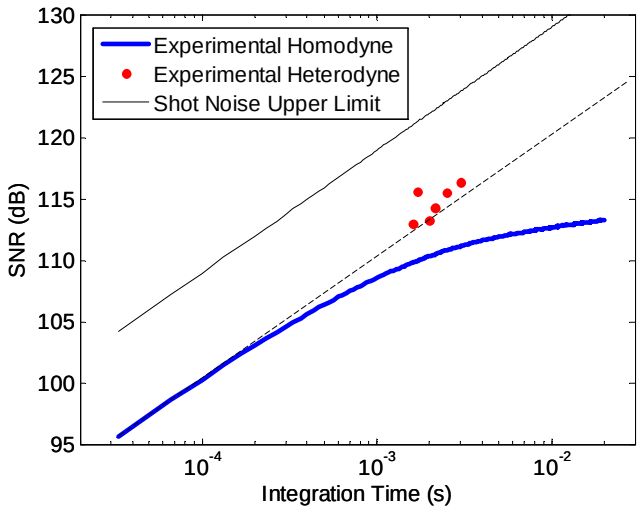

Fig. 8. A comparison of homodyne (blue) and heterodyne (red) SNR versus integration time. The black curve represents the upper limit on SNR for shot noise limited signals. A line drawn through the initial portion of the homodyne curve intersects the heterodyne data (dashed line). This implies that the homodyne data is white noise limited for short integration times, after which 1/f noise becomes dominant.

4.3 Characteristic time

Using the noise model described in section 2, we were able to theoretically predict the characteristic integration time at which 1/f noise began to dominate. However, this calculation required f_{min}. To verify our choice of $f_{min}=1/T$, we fit the data in Fig. 7, sampled at 30 kHz for 1 second to an expression for SNR, including both 1/f and shot noise terms:

$$SNR = \frac{x_0^2 \tau^2}{\sigma_{X,pink}^2 + \sigma_{X,white}^2} \tag{14}$$

Here, $\sigma^2_{X,pink}$ and $\sigma^2_{X,white}$ are given by Eq. (9) and Eq. (10), respectively. Amplitude values contained in these equations, A_{white} and A_{pink}, were obtained from the power spectrum, as described in section 4.1. The only free variables in Eq. (14) are the total photon count rate, x_0, and f_{min}, contained in $\sigma^2_{X,pink}$. The fit can be seen in blue in Fig. 7. From this fit we determined a f_{min} of 1.1 Hz, which is approximately equal to 1/(T=1s). This result helps to confirm the validity of our model for making predictions about experimental results.

With confidence in our value of f_{min}, we used the theoretical noise model to predict the characteristic integration time at which 1/f noise became dominant. This time was determined as the time at which white noise and 1/f noise give an equivalent noise variance, and the following equation holds:

$$\frac{A_{white}\tau}{2} = \int_{\omega_{min}}^{\infty} \frac{A_{pink}}{2\pi^2 f^{\alpha+2}} \left[1-\cos(2\pi f\tau)\right] d\omega \tag{15}$$

We calculated this characteristic time to be $\tau_{white\text{-}to\text{-}1/f}$ =1.65 ms, and note that the SNR of the measurement should begin to be affected at shorter times when 1/f noise is less than, but not negligible compared to white noise. This time agrees fairly well with our experimentally determined time of 2.1 ms.

#78143 - $15.00 USD Received 18 December 2006; revised 13 March 2007; accepted 13 March 2007

4.4 1/f noise power dependence

In the initial analysis we arrived at an expression for the variance of the noise amplitude distribution in terms of constants A_{pink} and A_{white}. For shot noise, the constant can be determined using knowledge of Poisson statistics. One question that arises concerns the form of the constant for 1/f noise, A_{pink}. Figure 9 shows the dependence of 1/f noise on reference arm power. These noise values were computed using an integration time of τ=10 ms, which falls well above the point at which 1/f noise becomes dominant in Figs. 7 and 8. The linear trend in Fig. 9 makes intuitive sense; like shot noise, the 1/f noise is directly proportional to the number of detected photons.

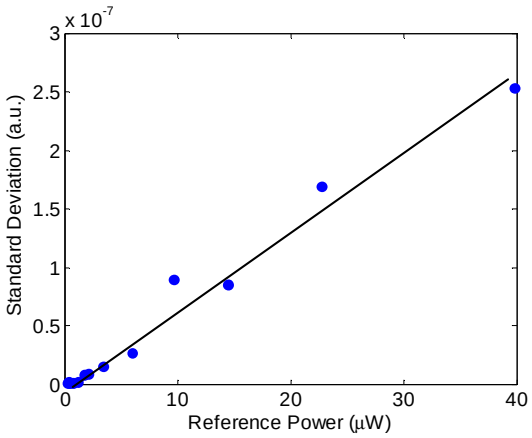

Fig. 9. The form of the 1/f noise amplitude [A_{pink} in Eq. (10)] is unknown, although we might expect it to depend on the reference arm power in some fashion. The blue dots represent experimental measurements and the black line is a linear fit to the data. The amplitude was found to follow a linear trend versus reference arm power, similarly to the shot noise amplitude.

4.5 Sources of 1/f noise

Finally, we examined the contribution of the photodetectors to 1/f noise in the interferometric system. We expect a different set of photodetectors to have different 1/f characteristics, and possibly different exponents, α. The initial detectors (New Focus #2011) showed a linear trend of α=1.40, while the replacement detectors (Thorlabs #DET10C) displayed an increase to α=2.17. The power spectra are plotted in Figs. 10(a) -10(b). We expect the shot noise limited SNR curve to be similar between both sets of detectors since the photon count rate remained the same. Using the results of our theoretical analysis plotted in Figs. 2 and 3, we expect that 1/f noise with a higher exponent will intersect the shot noise curve at a shorter integration time. These expectations are verified by comparing the experimental SNR versus integration time for the two sets of detectors. Although the two curves look very similar in the shot noise regime, the signals from Thorlabs detectors begin to shift from a linear shot noise curve to a flat 1/f noise curve almost an order of magnitude earlier than those of the initial photodetectors. These results emphasize the importance of careful detector selection in minimizing 1/f noise for optical systems.

In addition to detector noise, there is a component of the 1/f noise that arises from the light source. A portion of the noise was removed by subtracting the detected signal at D_4 from the signals at the other three ports. When this subtraction was not performed, we found a difference in SNR similar to that displayed in Fig. 10(c) where 1/f noise caused the SNR curve to flatten out at shorter integration times. This result was less dramatic than that in Fig. 10(c), with a maximum difference of approximately 3 dB between the data that had and had not been corrected using the signal from D_4. We note that this type of correction, commonly used to reduce excess intensity noise [14], is also an important factor in reducing 1/f noise.

#78143 - $15.00 USD Received 18 December 2006; revised 13 March 2007; accepted 13 March 2007

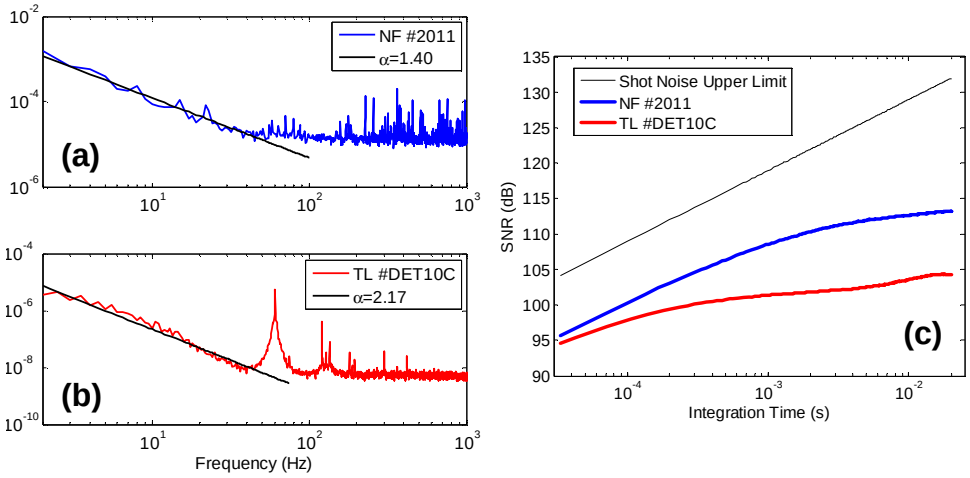

Fig. 10. Power spectra of initial detectors (a), and replacement detectors (b), showing a notable increase in the 1/f noise exponent, α. c) SNR versus integration time for both sets of detectors. The larger 1/f exponent of the Thorlabs detectors (TL #DET10C) caused 1/f noise to become a dominant process for shorter integration times than was seen in the New Focus detectors (NF #2011).

5. Conclusions

In conclusion, we have presented what is, to the best of our knowledge, a novel time domain method for analysis of the dependence of the noise variance on the integration time of the detection system. While we used this model to investigate 1/f noise in a homodyne interferometry system, it is applicable for any optical detection scheme in which the power spectrum of the noise fluctuations is known. We confirmed the validity of our model by demonstrating that our results are consistent with the well known dependence of white noise on integration time. The solutions to our model were found to be dependent on a minimum frequency, f_{min}, which was inversely related to the total time frame of the experiment. By restricting this total time frame it is possible to exclude large amplitude, low frequency components from the acquired signal. Our analysis revealed that the variance of the 1/f noise amplitude distribution shows two distinct regimes. For $0<\alpha<1$, the noise variance is dependent on $\tau^{\alpha+1}$, representing a transition from white noise to 1/f noise. However, for $\alpha>1$, the noise variance is dependent on τ^2, implying that when the dominant noise processes display a 1/f characteristic, the SNR of the measurement is constant versus integration time. The presence of both white and 1/f noise sources suggests the existence of a characteristic integration time, beyond which 1/f noise dominates and the SNR can no longer be significantly improved by increasing integration time.

We experimentally characterized the 1/f noise of our homodyne interferometer, finding a 1/f exponent of $\alpha=1.39 \pm 0.1$ and a 1/f noise corner of approximately 70 Hz. Experimental data confirmed our theoretical results, showing that the measured SNR tapers to a constant value in the 1/f regime. For short integration times, white noise processes were dominant. We have established white noise limited detection for short integration times by comparing our homodyne SNR to the SNR of the corresponding heterodyne interferometer, as well as to theory. Our experimental results demonstrated a characteristic integration time for our homodyne OCT interferometer, of $\tau_{white\text{-}to\text{-}1/f}$ =2.1 ms, beyond which increases in integration time did not produce corresponding increases in SNR. This time agrees fairly well with the theoretically determined value of $\tau_{white\text{-}to\text{-}1/f}$ =1.65 ms based on the measured power spectral characteristics of system. This characteristic time depends on the 1/f characteristics of the optical system, and is both system and detector dependent. Finally, we note that careful

#78143 - $15.00 USD Received 18 December 2006; revised 13 March 2007; accepted 13 March 2007

photodetector selection and characterization is important in order to minimize 1/f noise in homodyne detection.

Acknowledgments

This work was supported by a NSF Career Award, BES-0547657. E. J. McDowell acknowledges support from an NIH Ruth L. Kirschtein NRSA fellowship, EB006694.

#78143 - $15.00 USD Received 18 December 2006; revised 13 March 2007; accepted 13 March 2007